Chapter 19

FORCE MICROSCOPY, NANOCHEMISTRY AND NANOFABRICATION

RICARDO GARCIA*, MARCO CHIESA and YU KYOUNG RYU
Instituto de Ciencia de Materiales de Madrid, Consejo Superior de Investigaciones Científicas (CSIC) C/S or Juana Inés de la Cruz, 3 28049 Madrid, Spain

1. Introduction

Scanning probe microscopy (SPM), in particular atomic force microscopy (AFM), is a key tool in nanoscience and nanotechnology because of its ability to image at sub-10 nm resolution a wide variety of surfaces ranging from biomolecules to integrated circuits.[1–7] Furthermore, the performance of the instrument is not compromised by the surrounding medium. High resolution images are achieved in air, liquid or vacuum. A force microscope can be easily transformed into a modification tool by varying the relevant tip-surface interaction. This process has given rise to a large variety of atomic and nanometer-scale modification approaches.[8–10] Those approaches involve the interaction of a sharp probe with a local region of the sample surface and the variation of one or several parameters. Mechanical, thermal, electrostatic and chemical interactions, or some combinations among them, are exploited to modify molecules, nanostructures or surfaces with probe microscopes (Fig. 1). In the process, a variety of functional nanoscale patterns, data storage applications and nanomechanical and nanoelectronic devices have been developed.[9,11,12]

The scanning probe microscopy modification and manipulation approaches range from the sophisticated control of attractive van der Waals forces to move atoms[13] to the use of the AFM tip as a knife to

*Corresponding author: r.garcia@csic.es

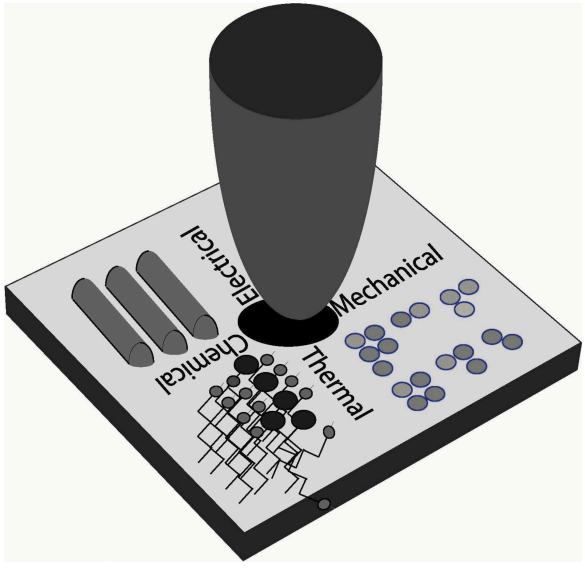

Fig. 1: Scheme of some of the mechanisms involved in tip-based nanofabrication.

scratch surfaces;[14,15] from the selective oxidation of a metallic surface to create thin insulating barriers[16] to the fabrication of quantum devices by modifying the electron gas density;[17] from the thermo-plastic deformation of polymers for three-dimensional patterning[18] to the fabrication of templates to build molecular architectures.[19]

This chapter is devoted to introducing some of the AFM methods based on the control of a chemical reaction to modify and/or pattern surfaces with nanoscale accuracy. The small size of the AFM tip's apex is often used to confine a variety of chemical reactions and/or physical processes. In some cases, the AFM probe acts as a carrier of molecules that, upon mechanical contact with the surface, will be transferred to the sample surface to form new chemical bonds. In other cases, an electric field is the driving force that promotes the field-induced evaporation of atoms from the tip. Other processes are mediated by the presence of a liquid meniscus which provides both the chemical species and the spatial confinement for a chemical reaction to occur. Finally, in some cases a hot tip facilitates the breaking of chemical bonds on certain polymer surfaces.

The relationship between AFM and nanochemistry was initially motivated and strengthened by nanopattering and nanofabrication applications. However, some recent examples, such as the exploration of new ways to decompose carbon dioxide, expand this relationship to other contexts.[20]

2. Field-induced Chemistry

Unusual chemical reactions have been observed in the presence of very high electric fields ~10–50 V/nm with field ion microscopes.[21,22] Those fields are of the same order of those inside atoms and molecules. Consequently, they are strong enough to induce the rearrangement of molecular orbitals leading to new chemical reactions. This has led to the existence of a field-induced chemistry. A force microscope interface offers a precise control and manipulation of high electric fields by changing the tip-surface separation and/or the voltage (Fig. 2). In contrast to field-ion microscopy that operates in ultra-high vacuum, the AFM experiments can be performed in ambient or liquid environments, which increases the number of available chemical species. Remarkably, high electric fields can be achieved in AFM by applying moderate voltages.

The electric field between two flat conducting surfaces separated by a distance D can be estimated as $F = V/D$. The presence of a sharp probe introduces a correction factor to the above expression. For a hyperboloidal tip, the field at the tip's apex is[23,24]

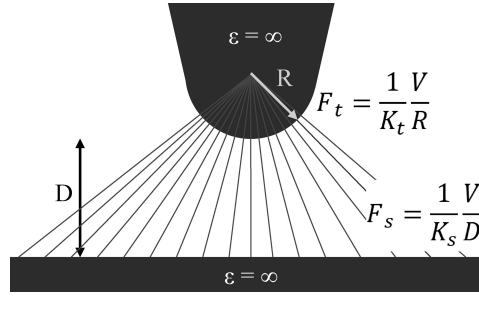

Fig. 2: Electric field between an AFM tip of radius R and a flat surface separated by a distance D. A radial distribution is assumed.

$$F_{\mathrm{t}} = \frac{1}{K_{\mathrm{t}}}\frac{V}{R} \tag{1}$$

while at the flat surface

$$F_{\mathrm{s}} = \frac{1}{K_{\mathrm{s}}}\frac{V}{D} \tag{2}$$

where K_t and K_s are geometrical factors. If $R \ll D$, it is deduced,[24]

$$K_{\mathrm{t}} \approx K_{\mathrm{s}} = \frac{1}{2}\ln\frac{4D}{R} \tag{3}$$

where V is the applied voltage and R is the probe radius. $K_{\mathrm{t}} \cong 2$ and $K_{\mathrm{s}} \cong 3$ are some values representative of many AFM experiments. In a force microscope interface the field can be easily determined and varied by either modifying the tip-surface distance or the voltage. Since the tip-surface separation is in the nanometer or sub-nanometer range, very high fields (1–30 V/nm) can be generated in the presence of tens of volts. In the presence of a gas, liquid, or solid material, those fields could be used to promote the evaporation of atoms from the tip, the breaking of chemical bonds in the molecules of the surrounding environment or the formation of new products. The control and manipulation of electric fields at the nanoscale is the basis of the relationship between field-induced chemistry and nanofabrication.

3. Carbon Dioxide Dissociation

Carbon dioxide is quantitatively the most important anthropogenic greenhouse gas. Its estimated atmospheric lifetime is about 100 years. Carbon dioxide is very stable because of its high enthalpy of formation ~ –4.1 eV (–394 kJ/mol). The high electric fields that can be generated in an AFM interface could be used to investigate new methods to decompose carbon dioxide and transform it into a solid material. In this respect, Garcia *et al.* have demonstrated a method to capture and transform carbon dioxide gas into a solid material by applying voltage pulses to an AFM interface in a carbon dioxide atmosphere.[20,25] The process requires the application of

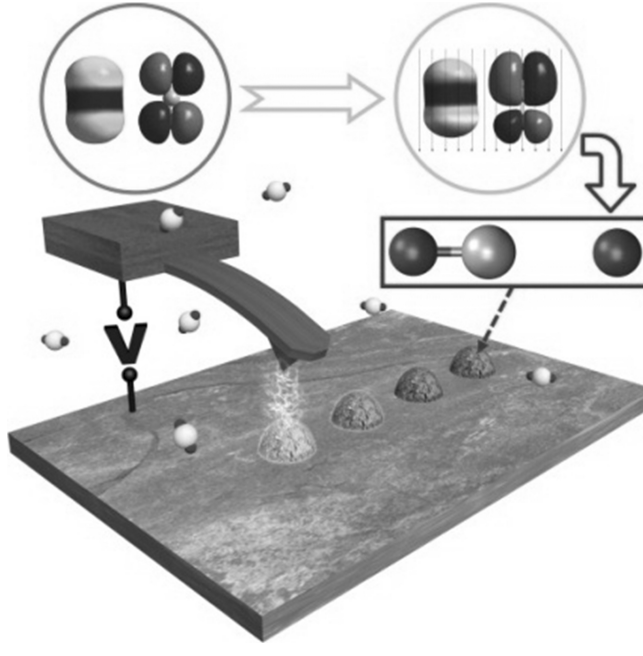

Fig. 3: Scheme of the electric field-induced dissociation of carbon dioxide molecules and subsequent generation of a carbonaceous pattern with an AFM probe.

low-to-moderate voltages ~10–40 V (Fig. 3). Interestingly, the activation of carbon dioxide by electric fields, which was first demonstrated with a force microscopy interface, could be up-scaled and generalized by using stamps patterned with billions of nanoscale asperities.

The transformation of CO_2 in the presence of an electric field can be separated into three major steps. The first step is the capture of the molecules into the gap region between the two electrodes. The second step is the activation of the molecules and the third step corresponds to the fabrication of a carbonaceous compound. The first step is a field-induced diffusion process.[26] The electric field polarizes the carbon dioxide and the resulting dipole moment interacts with the field. The potential energy of a CO_2 molecule under the influence of the field F can be approximated by

$$U = U_0 - \frac{1}{2}\alpha F^2 \tag{4}$$

where $\alpha = 2.93 \cdot 10^{-40}$ $C^2m^2J^{-1}$ is the static polarizability of CO_2 and U_0 is its free energy in the absence of the field.[27] Thus, in a non-uniform field, the molecule will experience a polarization force towards the conductive surfaces. The presence of high electric fields (0.1–30 V/nm) in the interface will trap the CO_2 between the conductive surfaces, and thus increase the gas density. We can estimate the change of pressure, p, between the electrodes as:

$$p = p_0 \exp(\Delta U / k_B T) \tag{5}$$

where p_0 is the pressure at zero field. For a field of 10 V/nm, we obtain $\Delta U = 92$ meV which in turns gives $p \approx 36 p_0$ (T = 298 K). The increase of pressure implies a higher collision rate between the gas molecules.

Quantum chemical calculations show that the field modifies the potential energy surface of dissociation into CO+O and shifts the energy of the molecular orbitals which leads to carbon dioxide splitting.[25] The field shifts the energy of the molecular orbitals and modifies the dipole moment. As the field increases, the molecular dipole moment builds up and different local charges form on the atoms. The carbon atom becomes more positive, while the charge difference between the two oxygen atoms increases. Also the two bond lengths become asymmetric (0.122 nm vs. 0.113 nm at 30 V/nm). The field also greatly affects the lowest unoccupied molecular orbital (LUMO), which becomes nearly degenerate with the highest occupied molecular orbital (HOMO) at 40 V/nm. At high fields, the HOMO becomes located outside the molecule, beyond O1. Closing the HOMO-LUMO gap promotes the detachment of the oxygen atom and the formation of two fragments. Calculations, at fields higher than 40 V/nm, show that the molecule spontaneously breaks down into CO+O. Concomitantly, the field affects a sigma molecular orbital, which becomes located on a CO fragment until it closely resembles the HOMO of carbon monoxide. Under these conditions, the products are charged and can easily react to form a solid, carbonaceous material, as it was confirmed by X-ray photoelectron spectroscopy (XPS).[20]

Scanning probe microscopes have also been used to investigate other types of carbon dioxide processes such as the photocatalytic dissociation of CO_2 on titanium dioxide surfaces.[28,29] These contributions show that the

process implies the adsorption of CO_2 molecules at oxygen vacancy defects of a TiO_2 (110) surface followed by the injection of one electron into the molecule, which has a barrier of 1.7 eV. The reorganization of the molecule leads to the dissociation of one C-O bond, with the oxygen atom healing the vacancy and the release of CO, with around 20–30% reabsorption at the Ti^{4+} site.

The high electric field in the proximity of the tip's apex has also been used to induce the evaporation[30,31] and/or ionization of a variety of materials.[32,33] The experiments involving ionization[32,33] have two steps: First, the molecules are ionized and ejected from a tip that is biased negatively (−6 V to −10 V); second, the ejected molecules are electrostatically attached to an attractive surface. The patterning can be switched on and off by applying a negative bias or by turning it back to zero, respectively. On the other hand, the dimensions of the patterns can be controlled by modulating the tip bias and the scanning speed. This method has been applied to deposit different kinds of organic materials, such as fullerenes, naphthalene or polymers, and inorganic materials such as gold on different substrates: HOPG (highly oriented pyrolytic graphite), graphite, ITO (indium tin oxide), or gold.

4. AFM Oxidation

AFM oxidation, also known as tip-based oxidation, nano-oxidation or local oxidation nanolithography, provides a remarkable example of the relationship between electric fields, nanochemistry and probe microscopy.[9] AFM oxidation is based on the spatial confinement of an anodic oxidation between the tip and the sample surface. In air, the oxidation process is mediated by the formation of a nanoscale water bridge (Fig. 4). The bridge acts as a nanoscale electrochemical cell. The tip is biased negatively (cathode) with respect to the sample surface (anode). AFM oxidation can be either performed with the tip in contact with the sample surface or in a non-contact mode.[34] In the latter case, the formation of a water bridge requires the application of a voltage. The non-contact AFM oxides are smaller and show higher aspect ratios under similar experimental conditions. Another advantage of the dynamic mode is that the tip suffers less wear and its lifetime is increased. This is an important point to

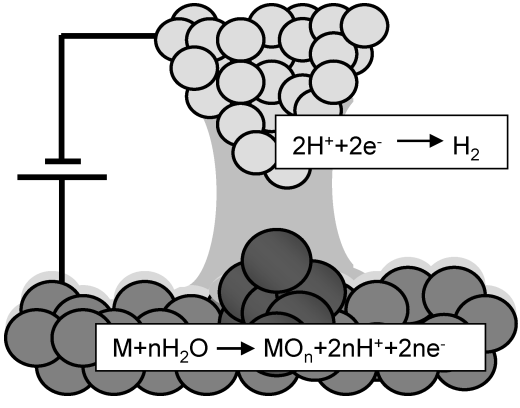

Fig. 4: Scheme of AFM oxidation highlighting the role of the water meniscus in the redox reactions at the tip-sample interface.

address pattern reproducibility. Tip-based oxidation started with the experiments performed with a scanning tunneling microscope (STM) by Dagata and co-workers.[35] However, the STM is rarely used today for local oxidation purposes because of the difficulties associated with its operation on poorly conductive surfaces.

In AFM oxidation, the electric field plays three roles: First, it induces the formation of a water bridge; second, it generates the oxyanions needed for the oxidation by decomposing water molecules; third, it drives the oxyanions to the sample interface and facilitates the oxidation process.

On silicon surfaces, the local oxidation process generates ultra-small silicon oxide nanostructures with a minimum lateral size of about 12 nm and a height that ranges from 1 nm to tens of nm depending on the oxidation conditions.[36–38] The height and the width of the oxide depend linearly on the voltage. The height h also shows a power law dependence with the pulse time t of the type

$$h \sim bt^{\gamma} \tag{6}$$

where γ is in the 0.1–0.3 range for Si(100) surfaces. Voltage pulse amplitudes and durations are, respectively, in the 10–30 V and 0.005–1 s ranges.

The role of the water meniscus is two-fold. It acts as a nanoscale electrochemical cell that provides the oxyanions thanks to which the reaction

takes place. In addition, it confines the reaction laterally, i.e., the size of the meniscus determines the resolution of the features obtained by this technique. During the redox process, the tip acts as the cathode, generating hydrogen:

$$2H^+(aq) + 2e^- \rightarrow H_2 \quad (7)$$

The anodic reaction occurs at the surface of the semiconductor or metallic substrate as following:

$$M + nH_2O \rightarrow MO_n + 2nH^+ + 2ne^- \quad (8)$$

The local oxidation process is accompanied by an extremely small faradaic current.[39] The current reflects the flux of O^- and OH^- ions between the tip and the surface. This current can be monitored *in situ* during the oxidation process. The current flow shows a quick increase upon liquid bridge formation (and tip approach). Then it begins to decrease while the oxide is being built. In the latter stage the current values are in the pico and sub-picoampere range.

The growth of nanostructures in AFM oxidation is space-charge-limited due to the liberation of ions during oxidation.[38,40,41] Dagata *et al.* suggested that for long oxidation times the residual trapped space charge is dominated by H_3O^+ ions.[40] However, for short pulse times, which are typically used in nanofabrication, Chiesa and Garcia observed that the residual space charge is negative, probably due to unreacted OH^- ions.[42] The residual space charge might have a considerable lifetime.[43] The existence of a negative charge within the oxides has been exploited to use the local oxides as templates for the organization of positively charged molecules, such as single-molecule magnets[44] and ferritin.[19]

The main parameters that control the local oxidation lithography process are the applied voltage (from a few volts to 20–30 V), the relative humidity (20%–80%), the duration of the process (10 μs–10 s), the tip-sample distance (2 nm–5 nm) and the scan speed (0.5 μm/s–mm/s). The presence of defects that are created during the growth of the oxide will also affect the final size of the patterns.

AFM oxidation has been used to fabricate a variety of nanoscale patterns and nanomechanical or nanolectronic devices. Figure 5 shows the steps to build some molecular architectures by combining AFM oxidation

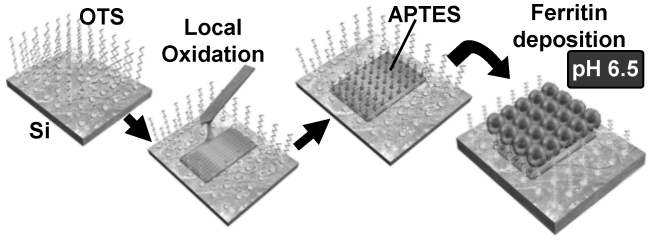

Fig. 5: Scheme of the main steps followed to obtain a ferritin pattern on a silicon surface by combining bottom-up electrostatic interactions and AFM oxidation. [Reprinted with permission from Ref. 19. Copyright © 2010 Wiley-VCH Verlag GmbH & Co. KGaA, Weinheim.]

and self-assembling methods. First, the silicon surface is functionalized with an octadecyltrichlorosilane (OTS) monolayer. This replaces the OH^- groups that dominate the native silicon surfaces in air with a methyl-terminated neutral surface. Then, a region of the functionalized surface is locally oxidized. The oxidation process removes the OTS monolayer. The sample is immersed in an aminopropyltriethoxysilane (APTES) solution until an APTES monolayer is deposited on the patterned region. The last step involves the deposition of the proteins. An example of the above process is the deposition of single molecules of ferritin on silicon surfaces with an accuracy similar to the size of the molecules (~10 nm).[19] The AFM images of the nanostripes before and after the deposition of ferritin molecules are shown in Fig. 6. There is a total absence of ferritin molecules outside the patterned stripes. This result underlines the strong selectivity of the patterning process.

Sophisticated nanolectronic devices such as silicon nanowire (SiNW) transistors and circuits have been fabricated by AFM oxidation nanolithography.[12,45,46] In this application, AFM oxidation generates a narrow oxide mask on top of the active layer of a silicon-on-insulator substrate. The unmasked silicon layer is then removed by using wet or dry etching. The local oxide protects the underneath silicon from the etching. This leaves a single-crystalline silicon nanowire (SiNW) with a top width that matches the width of the oxide mask. SiNWs with a channel width of 4 nm have been fabricated.[12] These types of nanoelectronic transistors have been used to develop very sensitive biomolecular sensors.[46]

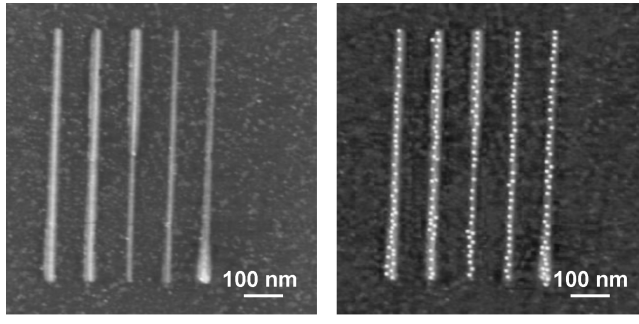

Fig. 6: (a) Silicon oxide nanostripes fabricated by AFM oxidation. (b) Selective deposition of ferritin molecules on the AFM oxidation pattern. [Reprinted with permission from Ref. 19. Copyright © 2010 Wiley-VCH Verlag GmbH & Co. KGaA, Weinheim.]

Silicon and titanium are the most used materials to perform local oxidation experiments; nonetheless, local oxidation has been extended to other interesting materials such as SiC[47] or graphene.[48] Xie *et al.* reported that the oxide grown on SiC was at least four times thicker than the one grown on Si under the same growth conditions. They attributed this result to an anisotropic diffusion of OH^- ions along polar and nonpolar directions in SiC during the process of oxidation.[47] Rolandi *et al.* applied AFM local oxidation to fabricate 35-nm-wide MoO_3 lines on an ultrathin molybdenum film deposited on a p-doped Si(100) substrate.[49] The MoO_3 patterns were etched away by simply dipping the sample in water with a high selectivity without affecting the Mo metal film.[49] The gaps left after the first wet etching served as masks patterns to fabricate Ti nanowires.

5. AFM Oxidation and Constructive Nanolithography

Selective oxidation of self-assembled monolayers (SAMs) has also been accomplished by AFM oxidation.[50–54] Two regimes can be distinguished when AFM oxidation is performed on surfaces functionalized with SAMs. For small and short voltage pulses (<8 V, ~1 ms) the oxidation is confined to the functionalized organic monolayer. Higher and longer voltage pulses cause the degradation of the initial monolayer and the anodization of the

underlying Si substrate.[53] The method has been applied to generate ring-like structures that have a core made of silicon oxide and a rim made of the SAM molecules.[52]

Sagiv and collaborators applied the AFM oxidation of SAMs to build molecular architectures.[51,55–57] They also explored some strategies to upscale the AFM fabrication process by using stamps.[55–57] First, they showed how an electrically biased tip could oxidize an OTS monolayer on a Si substrate. This modification step served as a template to deposit other organic layers. This method was called "constructive nanolithography" because of its additive character. Furthermore, the process does not imply changes of the underneath Si surface (see above). The technique was also applied to pattern mm^2 areas by replacing the AFM tip with a TEM grid which served as a conductive stamp.[55] They called this process "constructive microlithography". A variation of constructive microlithography has been applied to generate metallic micro/nano patterns.[57] First, a stamp made of a silver film deposited on an OTS/Si substrate is put in contact with a target surface. The target surface is made of an OTS monolayer on Si. This surface was previously patterned by AFM oxidation lithography. Then, by biasing the stamp positively with respect to the target, the silver ions are transferred selectively on the chemically activated –COOH terminals of the electrooxidized OTS (OTSeo). In this process, the adsorbed water layer acts as an electrolyte. The scheme of the fabrication process and the resulting pattern are described in Fig. 7. This method combines bottom-up and top-down nanofabrication processes and has the potential to generate complex interfaces.

6. Chemistry Beyond Water Bridges

We have described some of the properties of nanoscale water menisci to confine the lateral extension of the anodic oxidation. The availability of water molecules in air environments made the use of water bridges the obvious choice to explore nanochemistry with AFM. However, the AFM can be used to form and manipulate nanometer-size liquid bridges of polar and non-polar organic solvents such as ethyl alcohol, hexadecane, octane and 1-octene with a dynamic force microscope.[41,58–61] Tello and Garcia observed that the growth rate of the patterns increased significantly when

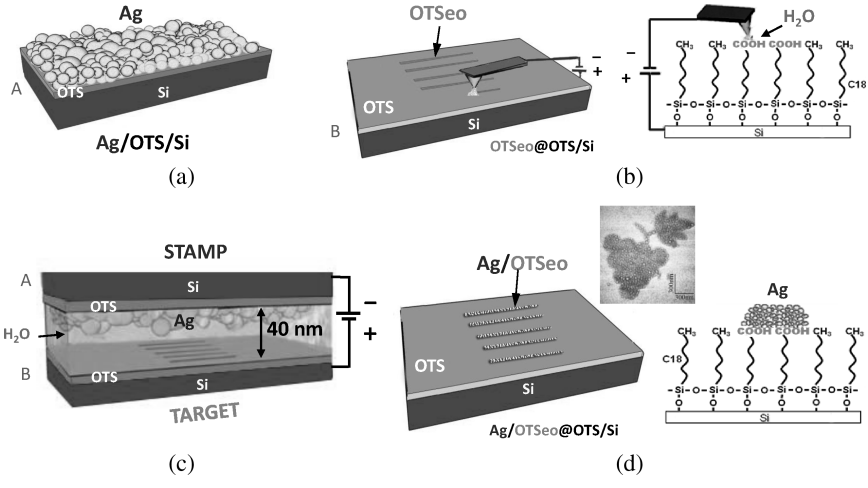

Fig. 7: Parallel contact electrochemical patterning and transfer (CEP-CET) process scheme. (a) The stamp (A) consists in an Ag layer deposited on a OTS@Si substrate. (b) A pattern is defined on the target substrate (B) by AFM oxidization. (c) Material is transferred from the stamp (A) to the target (B) when they are brought into contact. Typical parameters of the process are 3 V, 2 min, 100 N and RH 100%. (d) Final pattern: Ag has been deposited only on the chemically active OTSeo. An AFM phase image of one of the nanostructures fabricated by this method is shown. [Adapted from Ref. 57. Copyright © 2012 Berson *et al.*]

the process was performed in ethyl alcohol.[58] Initially, they attributed this enhancement to a decrease of the charged defects created during the oxidation process.[58] However, further experiments showed that the generated structures were not removed by exposition to HF vapors. This result questioned the silicon oxide nature of the fabricated structures. XPS spectroscopy measurements showed the presence of carbon sp^2 bonds which was attributed either to the formation of graphite or to the polymerization of carbon chains.[59] Consequently, the chemical composition of the liquid bridge does affect the composition of the fabricated nanostructures. Experiments performed in the presence of octane vapors also showed a faster growth rate with values of b and γ (see Eq. 6) higher than those found with water bridges.[61] Those values suggested a non-electrochemical process where the formation of nanostructures is a two-step process, condensation of the octane molecules in the vicinity of the AFM tip followed by the polymerization of the hydrocarbon chains induced by the strong electric field. Spectroscopy measurements enabled to propose that the

organic deposits are made by the polymerization and cross-linking of the CH_3-$(CH_2)_6$-CH_3 molecules.[62] This process was field-induced by the extremely high electrical field present at the interface, which has a mean value of about 10 V/nm, with peaks of up to 25 V/nm.

However, the process is not general. For example, Kinser *et al.*[41] found that when they performed local oxidation on a H-passivated Si(111) surface with both the tip and the substrate immersed in hexadecane, the organic solvent environment did not affect the growth kinetics nor the chemical nature of the patterned structures. On the other hand, Suez *et al.*[60] made further studies of scanning probe lithography in hexadecane, observing that while field-induced oxidation performed on a hydrophilic silicon surface yielded silicon oxide features, patterning on a hexamethyldisilazane (HMDS) hydrophobic surface gave rise to carbonaceous structures. Similarly, experiments performed with 1-octene showed kinetic parameters comparable to those obtained in water. Those values indicate an electrochemical process similar to field-induced oxidation. This conclusion was supported by the fact that the structures generated in 1-octene were readily etched by HF vapors, a property of silicon oxides.[62]

7. Deposition of Semiconductors

By immersing the AFM tip in a liquid cell filled with an organometallic compound, Rolandi and collaborators showed that it was possible to deposit a carbon-free semiconductor material onto a substrate with a controlled shape.[63–64] They used diphenylgermane to fabricate germanium nanostructures.[63] The experiments were performed by applying low-to-moderate voltages in the range of 0–20 V (the sample is biased positively) which generate high electric fields of about 10^9 V/m. The electric field fragments the diphenyl molecule into benzenes, which are dissolved in the liquid, and ionic germanium that is reduced on the surface forming germanium features. The germanium structures are not contaminated by any carbonaceous species. The versatility of this method has been further demonstrated with the use of diphenylsilane to create complex Si, Ge and SiGe nanostructures[64] in both serial (AFM) and parallel (stamp) patterning approaches (Fig. 8).

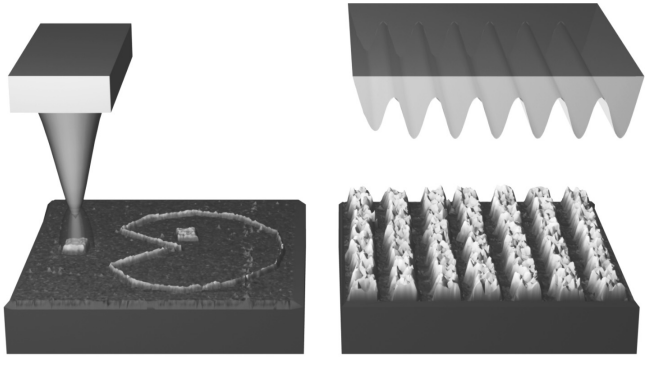

(a) (b)

Fig. 8: (a) Serial direct-write of Si and Ge from an organic precursor. The Ge PacMan was written at +12 V (sample) and 1 μm s^{-1}, the Ge eyeball was written at +11 V (sample) and 1 μm s^{-1}, the Si pellet on the left was written at +12 V (sample) and 5 μm s^{-1}. (b) Parallel direct write by using a gold-coated polydimethylsiloxane (PDMS) stamp. [Reprinted with permission from Ref. 64. Copyright © 2011 American Chemical Society.]

8. Thermal-Induced Nanoscale Chemistry

A heated tip has been used to induce mechanical and/or chemical transformations on polymeric molecules.[65–78] This method is very reproducible and reliable for patterning purposes. Depending on the chemical composition of the polymer (resist), the combination of a hot tip with a mechanical force produces either physical or chemical transformations in the resist which give rise to the formation of a hole in the polymer layer. The width and depth of the nanostructures depend on the tip's temperature, loading force and chemical composition of the polymer. The first experiments were performed by heating the tip with a laser pulse.[65] Those experiments generated patterns with features of 100–300 nm in width and 10 nm in depth. The alignment of the laser on the tip slowed down the patterning process which prompted the introduction of a Joule heating process by using a piezoresistive Si cantilever.[66] Piezoresistive cantilevers enable a higher degree of integration by using several of them in parallel. A parallel-writing prototype called "Millipede", based on 32×32 probe arrays (1024 cantilevers) was proposed in 1999.[67,68] The cantilevers are scanned

in the x and y directions simultaneously for writing/reading processes. They also share the same z-feedback control. Each cantilever-tip of the array only writes and reads within its storage field. However, most of the heating power (about 80%) is lost through transfer from the cantilevers to the chip body. As a consequence, the tip has to be heated up to 400°C. For reading, the temperature is reduced to 350°C, in order to avoid degradation of the written patterns.

High density memories can be fabricated by thermomechanical nanolithography.[67–70] The temperature and the loading force applied by an AFM tip are controlled to locally soften and create indentations on a polymer surface, which represent a logical "0" or "1". The same tip can be used as a tool to write the bits and the sensor to read them. Figure 9 shows the operation of the thermal cantilevers for data writing. By using a 1-μm-thick, 70-μm-long, two-legged Si cantilevers, 40 nm bits with a 120 nm pitch were obtained on poly(methyl methacrylate) (PMMA).[67] Data storage densities of 840 Gb/in^2 have been achieved with the "Millipede" method.[69] Higher densities of 4 Tb/in^2 have been achieved by using a single tip.[70]

One of the problems of the patterns fabricated on films made of linear polymers is that they are very prone to wear out during the reading stage.

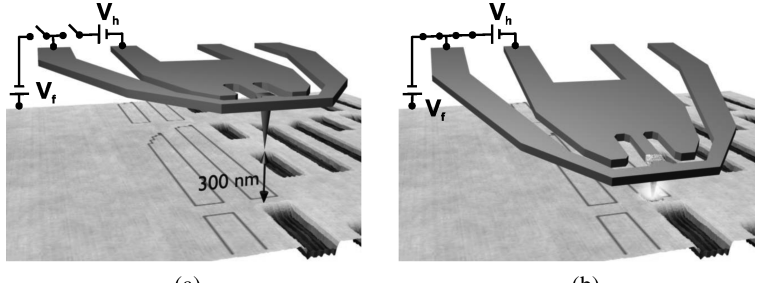

(a) (b)

Fig. 9: Principle of thermochemical nanolithography. (a) If no voltage is applied, the tip lays 300 nm above the sample surface. (b) By applying for a few microseconds the voltages V_h and V_f, which control the writing temperature and the electrostatic force, respectively, a pixel in the programmed bitmap is written on a molecular glass surface. [Reprinted with permission from Ref. 18. Copyright © 2010 American Association for the Advancement of Science.]

This could be solved by using cross-linked polymers which are more wear-resistant. However, the cross-linking process requires materials of higher glass transition temperature (T_g), which makes the thermal patterning more difficult. This has lead to the use of different materials such as Diels-Adler polymers,[71] unzip polymers[72] or molecular glasses.[18,73] For example, Diels-Adler polymers can be reversibly switched from a cross-linked state at low temperature to easily deformable dissociated fragments at high temperature.[71]

Basu *et al.*[74] applied a hot tip to cross-link locally the photoresist AZ5214E. The process transformed the resist as in a negative tone lithography fashion with a resolution comparable to the film thickness. Another example of nanoscale thermochemistry was the formation of carboxylic-terminated patterns on a block copolymer film for subsequent bioconjugation.[75] Sub-15 nm resolution was achieved in the thermoconversion of a hydrophobic polymer into a hydrophilic one.[76] A locally heated AFM tip has been recently used to locally desorb material from a glassy organic resist with a 15 nm half pitch; multistage processing allowed fabricating 3D structures which could be transferred to silicon by reactive ion etching.[18] Figure 10 shows the nanoscale replica of the Swiss mountain Matterhorn fabricated with this technique.

Thermochemical nanolithography has been performed on materials for (opto)electronics. An example is the fabrication of 28-nm-wide

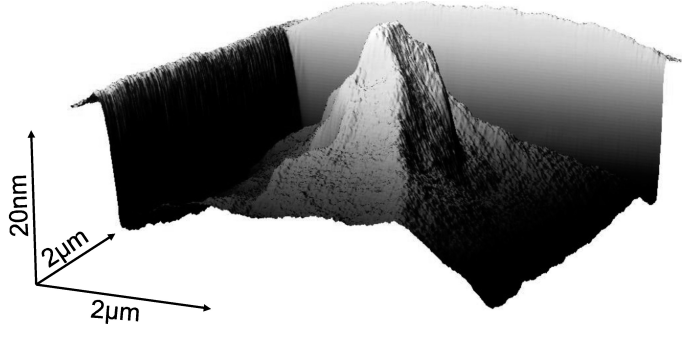

Fig. 10: Replica of the Matterhorn written into a molecular glass (3D data source: geodata © swisstopo) by AFM thermal removal of resist. The structure was written using 120 steps of layer-by-layer removal. [Reprinted with permission from Ref. 18. Copyright © 2010 American Association for the Advancement of Science.]

photoluminescent patterns of poly(phenylene vinylene) (PPV), by thermoconversion of its precursor poly(p-xylene tetrahydrothiophenium chloride) (PXT) by means of a heated Wollaston wire mounted on an AFM tip.[77] Another example is the fabrication of high mobility 12-nm-wide nanoribbons by local thermoreduction of oxidized epitaxial graphene films.[78]

9. Nanomachining and Mechanochemical Patterning

The most direct approach to modify a surface with an AFM tip is by applying a mechanical force to break atomic bonds and remove material from the surface.[14,15] However, this method has a poor pattern definition due to the tip's degradation and wear. The tip wear could be minimized by performing the experiments on materials more compliant than the tip. By nanoscratching a film of the conducting polymer mixture PEDOT:PSS (poly(3,4-ethylenedioxythiophene) poly(styrenesulfonate)), Li *et al.* were able to fabricate a pentacene field-effect transistor with a channel length of 50 nm.[79] However, spin-coated polymer films usually suffer from the pile-up of the removed material on the rims of the scratches. The pile-up implies a loss in pattern definition. This problem has been addressed by using polymer brushes.[80]

The application of nanomachining to alkylthiol self-assembled monolayers on gold has opened new patterning applications.[81,82] By controlling the applied force, it is possible to break the thiol-gold bond and selectively remove the SAM, and if the patterning is performed in the presence of another alkylthiol with a higher concentration and affinity, this molecule can replace the one removed by the tip. This approach could be called mechanochemical patterning and has two steps. The first step is called nanoshaving and the second nanografting. Recent applications include the immobilization of proteins on selected sites,[81] the fabrication of patterns of alternatingly charged thiols which could be resolved by measuring their surface potential,[83] or the positioning of single thiolated DNA molecules.[84] Obermair *et al.* proposed an electro-chemical version of the technique, where the AFM tip selectively removes a passivation layer and metals are electrochemically deposited from an electrolytic solution on the exposed areas of a gold electrode.[85]

10. Dip-pen Nanolithography

Aggregates of octadecanethiol were deposited onto mica after contact between tip and surface.[86] Those results opened the way to develop an AFM nanolithography based on the controlled transfer of molecules from the tip to a predefined location on the sample surface. This method was called "dip-pen nanolithography" by Mirkin and co-workers.[87–89] In this approach the molecules previously inked in the AFM tip are delivered to the surface via a liquid meniscus. Some of the first experiments were demonstrated by patterning alkanethiol self-assembled monolayers onto gold surfaces. Lately, the method has been extended to other molecules and systems that do not need the presence of sulphur-gold bonds. Arrays of cantilevers are now available to develop high-throughput parallel processes.[89] Recently, it has been shown that by varying the ink concentration and the dot size it is possible to control the number of deposited ferritin molecules.[90] One limitation of dip-pen nanolithography is the need to reconfigure the process depending on the substrate. Chen *et al.* showed that by using vapor-based coatings with adequate functional groups it was possible to deposit molecules with the same process on a large variety of substrates.[91]

An interesting electrochemical variation of dip-pen patterning is the proposal by Liu and collaborators.[92,93] In this case, metal salts are dissolved in the water meniscus formed between the tip and the substrate. When the appropriate bias is applied to the tip, the metal ions are reduced into metals and deposited on the surface. As in local oxidation lithography, the applied voltage and the relative humidity are two key factors in the fabrication process. This method has been utilized to modify locally a gallium nitride nanowire with a KOH-coated tip, obtaining a gallium nitride/gallium oxide heterostructure.[93]

11. Scanning Tunneling Microscopy and Nanochemistry

The scanning tunneling microscope (STM) was pivotal to discover the local anodic oxidation process on silicon surfaces.[35] This instrument has also been used to perform a variety of local chemical experiments with some patterning potential. For example, a monohydride layer on a silicon or germanium surface can act as a positive resist to perform STM lithography.

The tip is biased negatively with respect to the substrate and scanned locally over a delimited area of the passivated surface. If the electron energy exceeds the Si-H or the Ge-H bond strength, the hydrogen molecules are desorbed from the surface, thus leaving a pattern of clean Si or Ge.[94,95] The exposed areas can selectively undergo chemical modifications such as doping. By combining this method with epitaxial growth and electron beam lithography, Scappucci *et al.* fabricated phosphorous-doped Ge nanowires of 5 nm width.[95] Another example of STM applications in nanochemistry is the site-selective removal or exchange of self-assembled monolayers with a STM tip.[96–98] Frequently, the modification of SAMs with a STM tip is carried out with the aim of using the locally modified areas as nanotemplates or nanomasks previous to further patterning steps of a standard lithographic process. Gorman and co-workers have applied the above protocol to remove small areas of a dodecanethiol monolayer coated on gold, platinum and palladium substrates and to fill the empty sites with a different type of thiols.[97,98] The results showed that the bias required to desorb the first thiol layer and to replace it with the other SAM did depend on the underlying metal. This dependence was traced back to the different SAM-metal binding energies: palladium (3.1 V) less than gold (3.4 V) less than platinum (3.55 V). In all the three cases it was possible to obtain lines with lateral resolutions within the range of 10–15 nm.

Local electrochemistry has been applied to form metallic nanoclusters on metallic surfaces.[99–101] First, a metal such as copper is deposited on the STM tip by maintaining it at slightly negative values with respect to a Cu/Cu^{2+} reference electrode. Then the Cu-coated tip is approached to a gold surface to form a metallic neck. In the next step, the tip is retracted until the metallic neck is broken. This leads to the formation of a small metal cluster a few atomic layers thick. Depending on the applied voltage between tip and sample, tip-induced copper deposition, tip-induced copper dissolution or just surface imaging can occur.

12. Patterning Throughput

The serial character of force microscopy usually implies relatively slow processing times and consequently a low throughput for nanopatterning

applications. Improving throughput is addressed by two alternative approaches, the development of high speed AFM methods and the use of parallel arrays of cantilevers. Vicary and Miles developed a high-speed scan stage made of a quartz crystal tuning fork of 20 kHz as the fast-scan axis and a 15 Hz piezoelectric actuator perpendicular to it controlling the slow-scan direction. This high speed AFM has been applied to perform local oxidation patterns with 50 nm features at patterning speeds in the 1–10 cm/s range.[102,103] The use of some of the higher modes of the cantilever has also enabled fast thermomechanical patterning with a single tip.[104]

Some of the processes described above such as thermomechanical patterning,[67–69] local oxidation,[51,55,105] local electrochemistry or dip-pen nanolithography[89] are compatible with either the use of parallel arrays of cantilevers or with the use of stamps[106–110] that have predefined motives on them.[111–113] In particular the use of stamps represents an attractive approach to extend some of the properties found on AFM patterning to the millimeter scale.

13. Conclusions and Outlook

This chapter presents an overview of force microscopy-based nanopatterning methods where the formation of the nanostructures is mediated by a local chemical reaction. In particular we have discussed several processes such as AFM oxidation, field-induced chemical reactions, mechanochemical and thermomechanical patterning. In those methods the AFM has a dual role, first as a patterning tool and second as an instrument to control and study chemical reactions at the nanoscale. The technical requirements to transform an AFM to perform local chemical modifications are minimal so it will not be unlikely to find new applications in nanochemistry and nanofabrication.

Tip nanolithographies based on the spatial confinement of chemical reactions offer a relatively easy approach for the academic researcher to investigate chemical processes at the nanoscale and to fabricate sophisticated nanometer-scale devices. Some of the above applications are expected to experience a strong expansion in the near future.

Acknowledgments

We acknowledge the financial support from the Ministerio de Ciencia, Investigación e Innovación (MAT2009–08650) and the Comunidad de Madrid S2009/MAT-1467). Marco Chiesa acknowledges the program "Juan de la Cierva (MICINN)".

References

1. Garcia R, 2010. *Amplitude Modulation Atomic Force Microscopy*, Wiley-VCH, Weinheim.
2. Ando T, Uchihashi T and Fukuma T, 2008. *Prog Surf Sci* 83:337–437.
3. Gan Y, 2008. *Surf Sci Rep* 64:99–121.
4. Giessibl F J, 2003. *Rev Mod Phys* 75:949–983.
5. Gruverman A and Kalinin S V, 2006. *J Mater Sci* 41:107–116.
6. Barth C, Foster A S, Henry C R and Shluger A L, 2011. *Adv Mater* 23:477–501.
7. Brukman M J and Bonnell D A, 2008. *Phys Today* 61(6): 36–42.
8. Binnig G and Rohrer H, 1999. *Rev Mod Phys* 71:S324–S330.
9. Garcia R, Martinez R V and Martinez J, 2006. *Chem Soc Rev* 35:29–38.
10. Custance O, Perez R and Morita S, 2009. *Nat Nanotechnol* 4:803–810.
11. Pellegrino L, Biasotti M, Bellingeri E, Bernini C, Siri A S and Marré D, 2009. *Adv Mater* 21:2377–2381.
12. Martinez J, Martinez R V and Garcia R, 2008. *Nano Lett* 8:3636–3639.
13. Avouris P, 1995. *Acc Chem Res* 28:95–102.
14. Hsu J -H, Huang M-H, Lin H-H and Lin H-N, 2006. *Nanotechnology*, 17:170–173.
15. Tseng A A, 2011. *Small* 7:3409–3427.
16. Matsumoto K, Gotoh Y, Maeda T, Dagata J A and Harris J S, 2000. *Appl Phys Lett* 76:239–241.
17. Fuhrer A, Lüscher S, Ihn T, Heinzel T, Ensslin K, Wegscheider W and Bichler M, 2001. *Nature* 413:822–825.
18. Pires D, Hedrick J L, De Silva A, Frommer J, Gotsmann B, Wolf H, Despont M, Duerig U and Knoll A W, 2010. *Science* 328:732–735.
19. Martínez R V, Martínez J, Chiesa M, Garcia R, Coronado E, Pinilla-Cienfuegos E and Tatay S, 2010. *Adv Mater* 22:588–591.

20. Garcia R, Losilla N S, Martínez J, Martinez R V, Palomares F J, Huttel Y, Calvaresi M and Zerbetto F, 2010. *Appl Phys Lett* 96:143110.
21. Gomer R, 1993. *Field Emission and Field Ionization*, American Institute of Physics, New York.
22. Kreuzer H J, 1991. *Surf Sci* 246:336–347.
23. Smythe W R, 1952. *Static and Dynamic Electricity*, McGraw-Hill, New York.
24. Mesa G, Dobado-Fuentes E and Sáenz J J, 1996. *J Appl Phys* 79:39–44.
25. Calvaresi M, Martinez R V, Losilla N S, Martinez J, Garcia R and Zerbetto F, 2010. *J Phys Chem Lett* 1:3256–3260.
26. Tsong T T, 1991. *Phys Rev B* 44:13703–13710.
27. Maroulis G and Thakkar A J, 1990. *J Chem Phys* 93:4164–4171.
28. Lee J, Sorescu D C and Deng X, 2011. *J Am Chem Soc* 133:10066–10069.
29. Tan S, Zhao Y, Zhao J, Wang Z, Ma C, Zhao A, Wang B, Luo Y, Yang J and Hou J, 2011. *Phys Rev B* 84:155418.
30. Calleja M, Tello M, Anguita J, García F and García R, 2001. *Appl Phys Lett* 79:2471–2473.
31. Park K-H, Kim J, Ha J S and Song K-B, 2003. *J Vac Sci Technol B* 21: 1357–1360.
32. Liu J-F and Miller G P, 2007. *J Phys Chem C* 111:10758–10760.
33. Liu J–F and Miller G P, 2009. *Nanotechnology* 20:055303.
34. Tello M and Garcia R, 2001. *Appl Phys Lett* 79:424–426.
35. Dagata J A, Schneir J, Harary H H, Evans C J, Postek M T and Bennett J, 1990. *Appl Phys Lett* 56:2001–2003.
36. Calleja M and Garcia R, 2000. *Appl Phys Lett* 76:3427–3429.
37. Dagata J, Perez-Murano F, Martin C, Kuramochi H and Yokoyama H, 2004. *J Appl Phys* 96:2386–2392.
38. Dubois E and Bubendorff J-L, 2000. *J Appl Phys* 87:8148–8154.
39. Kuramochi H, Ando K, Tokizaki T and Yokoyama H, 2004. *Appl Phys Lett* 84:4005–4007.
40. Dagata J A, Inoue T, Itoh J, Matsumoto K and Yokoyama H, 1998. *J Appl Phys* 84:6891–6900.
41. Kinser C R, Schmitz M J and Hersam M C, 2006. *Adv Mater* 18:1377–1380.
42. Chiesa M and Garcia R, 2010. *Appl Phys Lett* 96:263112.
43. Baumgärtel T, Borczyskowski C V and Graaf H, 2012. *Nanotechnology* 23:095707.

44. Martínez R V, García F, García R, Coronado E, Forment-Aliaga A, Romero F M and Tatay S, 2007. *Adv Mater* 19:291–295.
45. Martinez R V, Martinez J and Garcia R, 2010. *Nanotechnology* 21:245301.
46. Chiesa M, Cárdenas P P, Otón F, Martínez J, Mas-Torrent M, García F, Alonso J C, Rovira C and García R, 2012. *Nano Lett* 12:1275–1281.
47. Xie X N, Chung H J, Xu H, Xu X, Sow C H and Wee A T S, 2004. *J Am Chem Soc* 126:7665–7675.
48. Weng L, Zhang L, Chen Y P and Rokhinson L P, 2008. *Appl Phys Lett* 93:093107.
49. Rolandi M, Quate C F and Dai H, 2002. *Adv Mater* 14:191–194.
50. Sugimura H and Nakagiri N, 1995. *Langmuir* 11:3623–3625.
51. Maoz R, Cohen S R and Sagiv J, 1999. *Adv Mater* 11:55–61.
52. Druzhinina T, Hoeppener S, Herzer N and Schubert U S, 2011. *J Mater Chem* 21:8532–8536.
53. Wouters D, Willems R, Hoeppener S, Flipse C F J and Schubert U S, 2005. *Adv Funct Mater* 15:938–944.
54. Wouters D and Schubert U S, 2007. *Nanotechnology* 18:485306.
55. Hoeppener S, Maoz R and Sagiv J, 2003. *Nano Lett* 3:761–767.
56. Zeira A, Chowdhury D, Maoz R and Sagiv J, 2008. *ACS Nano* 2:2554–2568.
57. Berson J, Zeira A, Maoz R and Sagiv J, 2012. *Beilstein J Nanotechnol* 3:134–143.
58. Tello M and Garcia R, 2003. *Appl Phys Lett* 83:2339–2341.
59. Tello M, Garcia R, Martín-Gago J A, Martínez N F, Martín-González M S, Aballe L, Baranov A and Gregoratti L, 2005. *Adv Mater* 17:1480–1483.
60. Suez I, Rolandi M, Backer S A, Scholl A, Doran A, Okawa D, Zettl A and Fréchet J M J, 2007. *Adv Mater* 19:3570–3573.
61. Martinez R V and Garcia R, 2005. *Nano Lett* 5:1161–1164.
62. Martínez R V, Losilla N S, Martinez J, Huttel Y and Garcia R, 2007. *Nano Lett* 7:1846–1850.
63. Torrey J D, Vasko S E, Kapetanovic A, Zhu Z, Scholl A and Rolandi M, 2010. *Adv Mater* 22:4639–4642.
64. Vasko S E, Kapetanović A, Talla V, Brasino M D, Zhu Z, Scholl A, Torrey J D and Rolandi M, 2011. *Nano Lett* 11:2386–2389.
65. Mamin H J and Rugar D, 1992. *Appl Phys Lett* 61:1003–1005.
66. Mamin H J, 1996. *Appl Phys Lett* 69:433–435.

67. Vettiger P, Brugger J, Despont M, Drechsler U, Dürig U, Häberle W, Lutwyche M, Rothuizen H, Stutz R, Widmer R and Binnig G, 1999. *Microelectron Eng* 46:11–17.
68. Vettiger P, Despont M, Drechsler U, Dürig U, Häberle W, Lutwyche M I, Rothuizen H E, Stutz R, Widmer R and Binnig G K, 2000. *IBM J Res Dev* 44:323–340.
69. Pantazi A, Sebastian A, Antonakopoulos T A, Bächtold P, Bonaccio A R, Bonan J, Cherubini G, Despont M, DiPietro R A, Drechsler U, Dürig U, Gotsmann B, Häberle W, Hagleitner C, Hedrick J L, Jubin D, Knoll A, Lantz M A, Pentarakis J, Pozidis H, Pratt R C, Rothuizen H, Stutz R, Varsamou M, Wiesmann D and Eleftheriou E, 2008. *IBM J Res Dev* 52:493–511.
70. Wiesmann D, Rawlings C, Vecchione R, Porro F, Gotsmann B, Knoll A, Pires D and Duerig U, 2009. *Nano Lett* 9:3171–3176.
71. Gotsmann B, Duerig U, Frommer J and Hawker C J, 2006. *Adv Funct Mater* 16:1499–1505.
72. Gotsmann B, Knoll A W, Pratt R, Frommer J, Hedrick J L and Duerig U, 2010. *Adv Funct Mater* 20:1276–1284.
73. De Silva A, Lee J-K, André X, Felix N M, Cao H B, Deng H and Ober C K, 2008. *Chem Mater* 20:1606–1613.
74. Basu A S, McNamara S and Gianchandani Y B, 2004. *J Vac Sci Technol B* 22:3217–3220.
75. Duvigneau J, Schönherr H and Vancso G J, 2008. *Langmuir* 24:10825–10832.
76. Szoszkiewicz R, Okada T, Jones S C, Li T-D, King W P, Marder S R and Riedo E, 2007. *Nano Lett* 7:1064–1069.
77. Fenwick O, Bozec L, Credgington D, Hammiche A, Lazzerini G M, Silberberg Y R and Cacialli F, 2009. *Nat Nanotechnol* 4:664–668.
78. Wei Z, Wang D, Kim S, Kim S-Y, Hu Y, Yakes M K, Laracuente A R, Dai Z, Marder S R, Berger C, King W P, de Heer W A, Sheehan P E and Riedo E, 2010. *Science* 328:1373–1376.
79. Li L, Hirtz M, Wang W, Du C, Fuchs H and Chi L, 2009. *Adv Mater* 22:1374–1378.
80. Hirtz M, Brinks M K, Miele S, Studer A, Fuchs H and Chi L, 2009. *Small* 5:919–923.
81. Hu Y, Das A, Hecht M H and Scoles G, 2005. *Langmuir* 21:9103–9109.
82. Liu M, Amro N A and Liu G-Y, 2008. *Annu Rev Phys Chem* 59:367–386.

83. Moores B, Simons J, Xu S and Leonenko Z, 2011. *Nanoscale Res Lett* 6:185.
84. Josephs E A and Ye T, 2010. *J Am Chem Soc* 132:10236–10238.
85. Obermair C, Wagner A and Schimmel T, 2011. *Beilstein J Nanotechnol* 2:659–664.
86. Jaschke M and Butt H-J, 1995. *Langmuir* 11:1061–1064.
87. Piner R D, Zhu J, Xu F, Hong S and Mirkin C A, 1999. *Science* 283:661–663.
88. Salaita K, Wang Y and Mirkin C A, 2007. *Nat Nanotechnol* 2:145–155.
89. Shim W, Braunschweig A B, Liao X, Chai J, Lim J K, Zheng G and Mirkin C A, 2011. *Nature* 469:516–520.
90. Bellido E, de Miguel R, Ruiz-Molina D, Lostao A and Maspoch D, 2010. *Adv Mater* 22:352–355.
91. Chen H-Y, Hirtz M, Deng X, Laue T, Fuchs H and Lahann J, 2010. *J Am Chem Soc* 132:18023–18025.
92. Li Y, Maynor B W and Liu J, 2001. *J Am Chem Soc* 123:2105–2106.
93. Maynor B W, Li J, Lu C and Liu J, 2004. *J Am Chem Soc* 126:6409–6413.
94. Lyding J W, Shen T-C, Hubacek J S, Tucker J R and Abeln G C, 1994. *Appl Phys Lett* 64:2010–2012.
95. Scappucci G, Capellini G, Johnston B, Klesse W M, Miwa J A and Simmons M Y, 2011. *Nano Lett* 11:2272–2279.
96. Ross C B, Sun L and Crooks R M, 1993. *Langmuir* 9:632–636.
97. Williams J A and Gorman C B, 2007. *Langmuir* 23:3103–3105.
98. Krämer S, Fuierer R R and Gorman C B, 2003. *Chem Rev* 103:4367–4418.
99. Ullmann R, Will T and Kolb D M, 1993. *Chem Phys Lett* 209:238–242.
100. Kolb D M, Ullmann R and Will T, 1997. *Science* 275:1097–1099.
101. Wei Y-M, Zhou X-S, Wang J-G, Tang J, Mao B-W and Kolb D M, 2008. *Small* 4:1355–1358.
102. Vicary J A and Miles M J, 2008. *Ultramicroscopy* 108:1120–1123.
103. Vicary J A and Miles M J, 2009. *Nanotechnology* 20:095302.
104. Paul P C, Knoll A W, Holzner F, Despont M and Duerig U, 2011. *Nanotechnology* 22:275306.
105. Minne S C, Adams J D, Yaralioglu G, Manalis S R, Atalar A and Quate C F, 1998. *Appl Phys Lett* 73:1742–1744.
106. Yokoo A, 2003. *Jpn J Appl Phys* 42:L92–L94.
107. Cavallini M, Mei P, Biscarini F and García R, 2003. *Appl Phys Lett* 83:5286–5288.

108. Martinez R V, Losilla N S, Martinez J, Tello M and Garcia R, 2007. *Nanotechnology* 18:084021.
109. Albonetti C, Martinez J, Losilla N S, Greco P, Cavallini M, Borgatti F, Montecchi M, Pasquali L, Garcia R and Biscarini F, 2008. *Nanotechnology* 19:435303.
110. Simeone F C, Albonetti C and Cavallini M, 2009. *J Phys Chem C* 113:18987–18994.
111. Mühl T, Kretz J, Mönch I, Schneider C M, Brückl H and Reiss G, 2000. *Appl Phys Lett* 76:786–788.
112. Farkas N, Comer J R, Zhang G, Evans E A, Ramsier R D, Wight S and Dagata J A, 2004. *Appl Phys Lett* 85:5691–693.
113. Yokoo A and Sasaki S, 2005. *Jpn J Appl Phys* 44:1119–1122.